Biomimetic silicification of demineralized hierarchical collagenous tissues

Li-na Niu[a]‡, Kai Jiao[a]‡, Heonjune Ryou[b], Anibal Diogenes[c], Cynthia K.Y. Yiu[d], Annalisa Mazzoni[e], Ji-hua Chen[a,*], Dwayne D. Arola[b], Kenneth M. Hargreaves[c], David H. Pashley[f], Franklin R. Tay[f,*]

‡These authors contributed equally to this work

*To whom correspondence should be addressed.

SUPPORTING INFORMATION

Table of Contents

S1: Materials and methords

Dynamic light scattering (DLS) and zeta potential. For particle size distribution and zeta potential measurement, 10% silicic acid solution was mixed with same volume of deionized water or 1.333 mM of PAH solution to produce 5% silicic acid solution (pH=3) and 0.667 mM PAH stabilized-5% silicic acid solution (PAH-SA, pH=5). One hour after sample preparation, particle size distribution and zeta potential of the 5% silicic acid solution and the PAH-SA solution were determined using a Zetatrac Particle Size Analyzer (Microtrac Inc., York, PA, USA), with deionized water as the carrier liquid. Samples (refractive index 1.49) were prepared in glass scintillation vials by diluting with deionized water (refractive index 1.333) at 3 vol% concentration. The pH value of deionized water used for dilution of the 10% silicic acid solution and the PAH-SA solution was adjusted to 3 and 5, respectively, to prevent the effect of pH change on premature polycondensation of silicic acid into amorphous silica. The sample chamber was filled with the respective acidified deionized water, which was used to produce a background measurement. The samples were added to the water in the chamber, and each diluted sample was run for 100 sec. The average particle diameter was determined in the intensity mode; measurements were taken in triplicates. Calculations were performed using the Microtrac FLEX application software, based on the particle refractive index and the carrier fluid refractive index.

Transmission electron microscopy (TEM). Silicified fish scale and bovine bone specimens were fixed in 2% glutaraldehyde, post-fixed with 1% osmium tetroxide, dehydrated in an ascending ethanol series (50-100%), immersed in propylene oxide and embedded in epoxy resin. Ninety nanometer thick sections were prepared and examined using a JSM-1230 TEM (JEOL, Tokyo, Japan) at 110 kV. All sections were examined without further staining. Images were recorded using a 4K x 4K Gatan CCD camera.

Scanning electron microscopy. Silicified fish scales after sintering at 700 ºC for 3 hours were sputter-coated with gold/palladium and examined using a field emission-scanning electron microscope (XL-30 FEG; Philips, Eindhoven, The Netherlands) operating at 10-15 kV.

Attenuated total reflection–Fourier transform infrared spectroscopy (ATR-FTIR). The fish scales before and after demineralization, and the silicified fish scales before and after sintering were desiccated with anhydrous calcium sulphate for 24 hours prior to spectrum acquisition. A Nicolet 6700 FT-IR spectrophotometer (Thermo Scientific, Waltham, MA, USA) with an ATR setup was used to collect infrared spectra between 4,000-400 cm^{-1} at 4 cm^{-1} resolution using 32 scans. An amorphous sol-gel silica reference (Ludox TM-50 colloidal silica, Sigma-Aldrich, St. Louis, MO, USA) was also used for comparison.

Scanning transmission electron microscopy-energy dispersive X-ray analysis (STEM-EDX). Elemental analysis of representative silicified bovine cortical and trabecular bone was performed on unstained, non-osmicated TEM sections, using a Tecnai G2 STEM (FEI, Hillsboro, OR, USA) at 200 kV. Spectrum acquisition and elemental mapping were conducted using an Oxford Instruments INCA x-sight detector. Images were collected with a Gatan 1K x 1K CCD camera. Elemental mappings were acquired with the FEI TIA software using a spot dwell time of 300 msec. As each

250 x 250 pixel mapping required 7 hours to complete, drift correction was performed after every 30 images.

Micro-computed tomography (Micro-CT). Silicified bovine cortical bone specimens were scanned non-destructively using a SkyScan 1174 X-ray micro-CT scanner (Micro Photonics, Allentown, PA, USA) with a 1-mm thick Al filter to remove low-energy radiation. Scanning was performed with a spatial resolution of 14.25 μm. Projection images were collected at 50 kV and 800 μA using 360º rotation, with 0.6º and 3 sec exposure time per projection step. Images were reconstructed using the NRecon software (Skyscan 1174, Kontich, Belgium) and a 20% beam hardening correction. Segmentation and visualization of the 3-D volume were performed using the DataViewer 2.0 and CTvox 2.4 software.

Solid-state nuclear magnetic resonance spectroscopy. Silicified bovine cortical bone specimens were pulverized in liquid nitrogen. Silicon solid-state NMR was performed at ambient temperature using a 270 MHz spectrometer (JEOL, Tokyo, Japan) equipped with a 7 mm Magic Angle Spinning (MAS) probe. Spectra were acquired in the $^{1}H \rightarrow {}^{29}Si$ cross polarization (CP) mode, using a MAS frequency of 4 kHz, with a 45 degree pulse angle of 5 μsec and a recycle delay of 3 sec. The ^{1}H Larmor frequency for ^{29}Si was 53.76 MHz. Chemical shifts were referenced to external tetramethylsilane at 0 ppm.

Powder X-ray diffraction. Silicified bovine bone samples were thoroughly rinsed with Milli-Q water for 10 times (5 min each time), air-dried, immersed in liquid nitrogen for 30 min, and pulverized to produce a fine powder. Additional silicified bovine bone samples were sintered in a box furnace (SentroTech Corp., Berea, Ohio, USA) to remove the organic phase. The temperature was raised from ambient temperature to 700 ºC at 10 ºC/min in atmospheric air, maintained at 700 ºC for 3 hours and cooled to room temperature at 10ºC/min. The remaining inorganic phase was similarly pulverized. X-ray diffraction (Rigaku America, Woodlands, TX, USA) of the non-sintered and sintered powders was performed using Ni-filtered Cu Kα radiation (30 KeV, 20 mA), in the 2θ range of 3-60°, with a scan rate of 4°/min, and a sampling interval of 0.02°. The phase composition was assigned by comparing the acquired spectra with peaks identified in the International Center for Diffraction Data database.

Thermogravimetric analysis. Thermogravimetric analysis was performed with a Q500 thermogravimetric analyzer (TA Instruments, New Castle, DE, USA). Approximately 15 mg of calcified bovine bone and silicified bovine bone were placed in individual platinum pans and heated at a rate of 10°C/min to 1000 °C in atmosphere air. The data were analyzed using the Universal Analysis 2000 software (TA Instruments) and expressed as weight *vs* temperature as well as derivative weight *vs* temperature.

Nanoscopical dynamic mechanical analysis (nanoDMA). NanoDMA indentations were performed on: calcified compact bone, decalcified compact bone, and silicified compact bone specimens. Indentations were made using a 400 μN static load with a dynamic load that is 5% of static load (20 μN). The loading frequency was 10 Hz. Complex (E*), storage (E'), loss (E") moduli and tanδ (Phase Angle, E"/ E') were calculated (N=15). Specimens were scanned in the hydrated

condition. Data obtained for the complex (E*), storage (E'), loss (E") moduli and tanδ were analyzed separately. Each data set was first evaluated for its normality and homoscedasticity assumptions prior to analysis with one-way analysis of variance (ANOVA) and post-hoc multiple comparison procedures (Holm-Sidak method). Statistical significance for all tests was pre-set at $\alpha = 0.05$.

S2: Hierarchical structure of natural fish scale

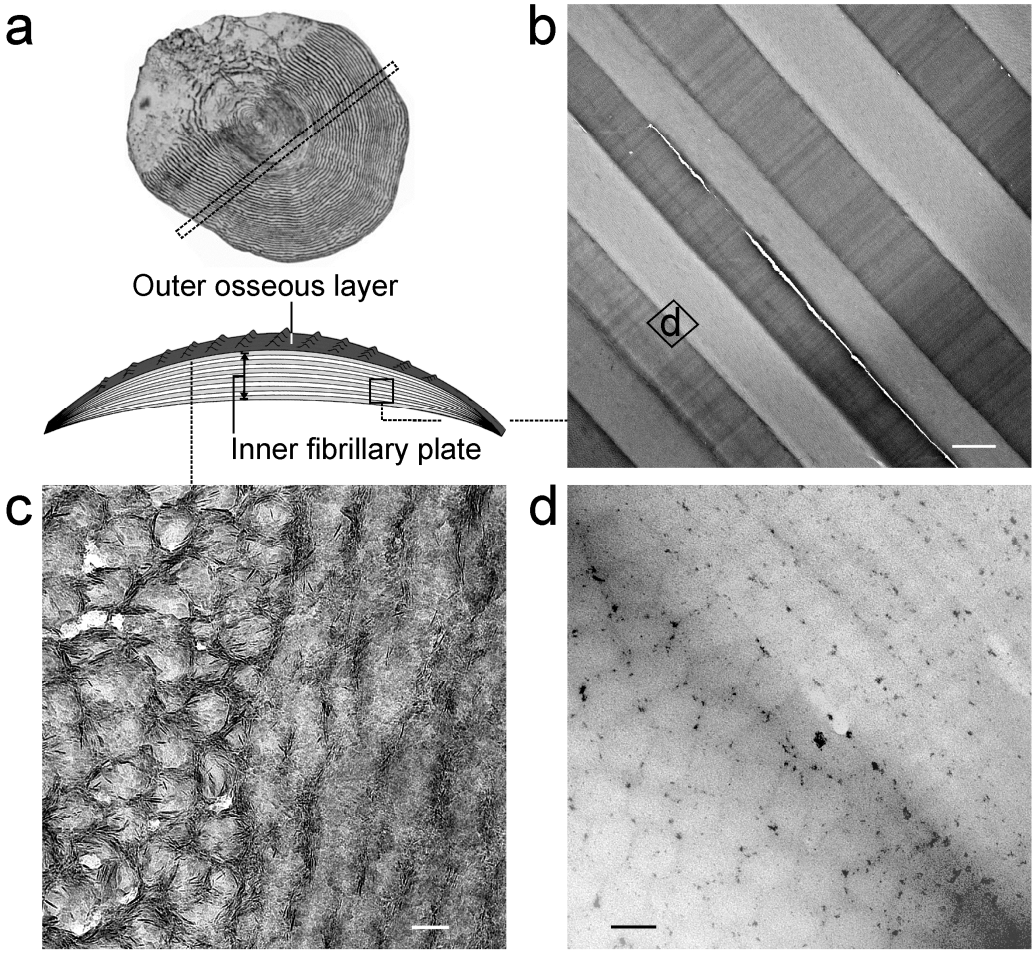

Figure S2. Unstained TEM images of undemineralized scales derived from *Cyprinus carpio* (common carp). **a**. Schematic representation of a carp scale, consisting of an outer highly-mineralized osseous layer and an inner fibrillary plate [S1]. **b**. Low magnification of the internal fibrillary plate that is made up of 15-20 plies of collagen. Each ply consists of 30-50 densely-packed collagen fibrils that are arranged parallel to each other. Collagen fibrils from one ply are arranged orthogonally to those in the next ply, yielding a plywood-like pattern (bar = 2 μm). **c.** High magnification of two sub-surface plies (oldest) beneath the surface osseous layer. Each ply contains highly-mineralized collagen fibrils with both intrafibrillar and extrafibrillar apatite deposits (bar = 100 nm). **d.** High magnification of an interior ply (youngest) adjacent to the fish body (box labeled "d" in Figure S1-b). Mineralization is sparse and located exclusively within the extrafibrillar spaces (bar = 100 nm).

S3: Poly(allylamine hydrochloride)-stabilized silicic acid

In vitro studies have shown that different kinds of polyamine analogs are able to stabilize polysilicic acid as a "soluble" silica phase by the formation of hydrogen bonds between the surface silanol groups of silica and the amine groups of the polyamine [S2-S6]. Such a process inhibits further condensation of the polysilicic acid due to reduction in availability of $\equiv$Si-O$^-$ anions that are active in nucleophilic reaction with monomeric $Si(OH)_4$ [S4,S6]. In the present study, poly(allylamine hydrochloride) was used to stabilize silicic acid as "soluble" silica particles.

A. *Effect of PAH concentration on gelling time of 5% silicic acid*

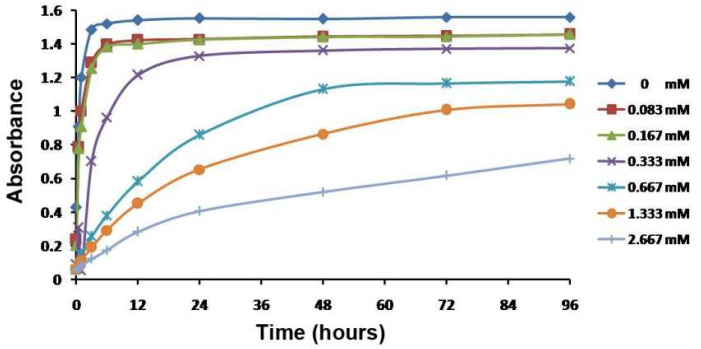

Figure S3-A. Changes in optical density profiles over time for 5% silicic acid containing different concentrations of poly(allylamine hydrochloride) (PAH) at pH 5. Each data point represents the mean of 9 measurements.

The results of the turbidity assay indicate that in the absence of PAH, 5% silicic acid gelled within 3 hours at pH 5. When 0.667 mM PAH was included in the silicic acid, gelling occurred after 48 hours. Decrease in absorbance of the gelled silicic acid with increasing PAH concentration is probably the result of reduced particle size of the PAH-stabilized soluble precursors associated with increasing PAH concentrations. The lowest PAH concentration that enabled the silicic acid solution to remain in a sol state for 48 hours was used to prepare PAH-stabilized silicic acid (PAH-SA)for biomimetic silicification. This provided sufficient time for the PAH-SA to infiltrate into dense natural collagen matrices. The silicifying medium was further replaced daily in subsequent experiments to prevent the sols from becoming too viscous during silicification of the natural collagen matrices.

B. *Particle size distribution and zeta potential measurement of 5% silicic acid and PAH-SA*

Particle size and zeta potential measurements of 5% silicic acid (pH=3) and PAH-SA (pH=5) were conducted 1 hour after preparation. The diameter of the particles was indicated as "Dia", which represents the mean diameter of 50% (D50) of the particles in each mode, after determining the minimum and maximum sizes contributing to the specific peak under consideration. For a solution that exhibited a multimodal distribution of particle sizes, each peak was represented by a separate D50 value. For a solution that exhibited a unimodal particle size distribution, the "Dia" was equal to 50% of the particle distribution. The "Vol%" value represented the percentage

contribution of each peak to the total volume of the distribution. For zeta potential, a mean value was obtained from three readings of each sample. The value represented the potential difference between the dispersion medium and the stationary layer of fluid attached to the dispersed particle. Zeta potential is related to colloidal dispersion stability. Zeta potential value greater than 25 mvolts (mV; positive or negative) is an indication of colloidal stability.

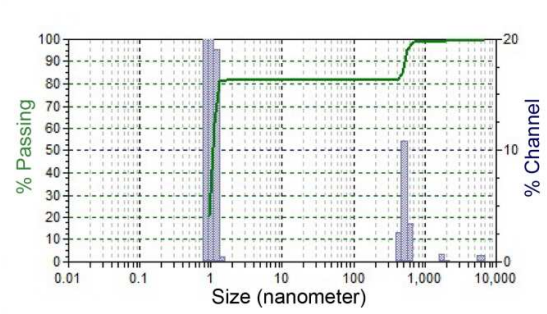

Peaks

Dia(nm)	Vol%
1996	1.4
539.0	15.7
1.050	82.9

Figure S3-B-a Bar graph of the particle size distribution (cumulative percentage) of 5% silicic acid.

A trimodal particle size distribution was observed for the 5% silicic acid at pH 3. There was a preponderance of smallest size particles (1.05 nm), with a vol% of 82.9%. Apart from the smallest particles, there were some large agglomerates present in the sample. They were thought to be incompletely hydrolyzed TEOS droplets. These droplets were removed by centrifuging in all subsequent experiments. The zeta potential of this solution was -38.95 ± 2.5 mV.

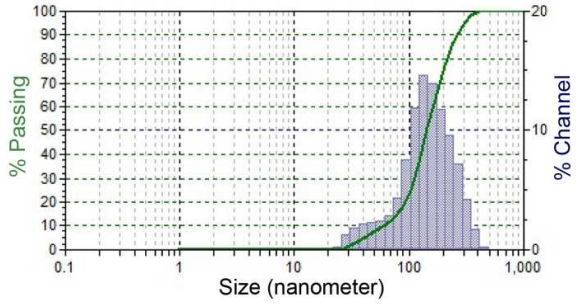

Peak

Dia(nm)	Vol%
142.2	100.0

Figure S3-B-b Bar graph of the particle size distribution (cumulative percentage) of poly(allylamine hydrochloride)-stabilized silicic acid.

For the 0.667 mM PAH-stabilized silicic acid, there was a unimodal particle size distribution, with D50 being 142.2 nm. The zeta potential of PAH-SA was 39.4 ± 3.0 mV, which means that particle dispersion in the solution was relatively stable. The positive charge on the PAH-SA complex is due to the protonation of PAH (pKa = 8.5) at pH 5 [S7].

S4: TEM examination of collagen sponges silicified without poly-allylamine (control I)

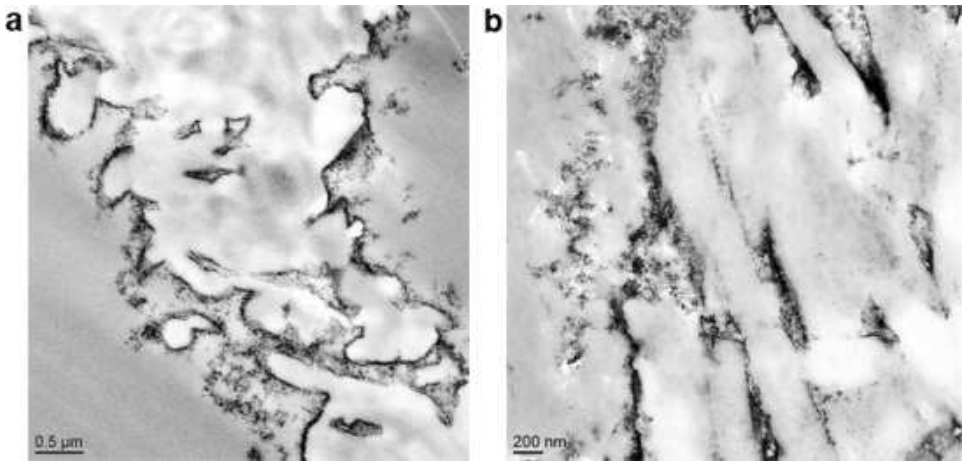

Figure S4 a. Unstained TEM image showing deposition of silica particles along the surface of a fiber leaflet (cross section) from a collagen sponge, after mineralization with 5% silicic acid in the absence of PAH (SA control). Each fiber consists of many collagen fibrils (bar = 0.5 µm). **b**. High magnification of similar silica particles deposited along the surfaces of individual collagen fibrils (bar = 200 nm). Banding of those fibrils was hardly identified as the specimen was osmicated only, without additional staining.

S5: Scanning electron microscopy of sintered, silicified fish scales

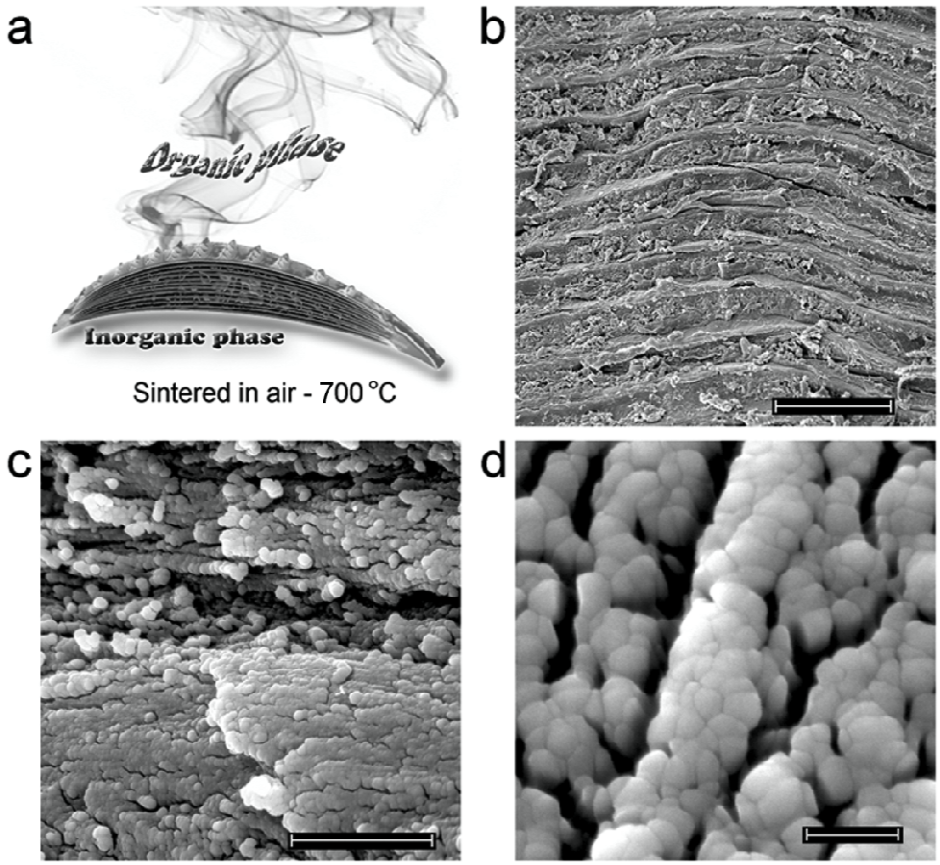

Figure S5. Scanning electron microscopy of sintered, silicified fish scales confirms intrafibrillar silicification. **a.** Schematic of sintering of a silicified fish scale to produce orthogonally-arranged layers of inorganic silica. **b.** Cross-sectional view of the silicified fish scale after sintering. The original lamellar structure of the fish scale was replaced by inorganic silica layers (bar = 50 μm). **c.** The sintered silica phase within a single ply (bar = 500 nm). **d.** High magnification of the fused silica phase, revealing ceramic-like, nanocrystalline characteristics (bar = 100 nm), which is caused by transformation of amorphous silica into crystalline silica phases at high sintering temperature.

S6 TEM of demineralized fish scales silicified without poly-allylamine (control II)

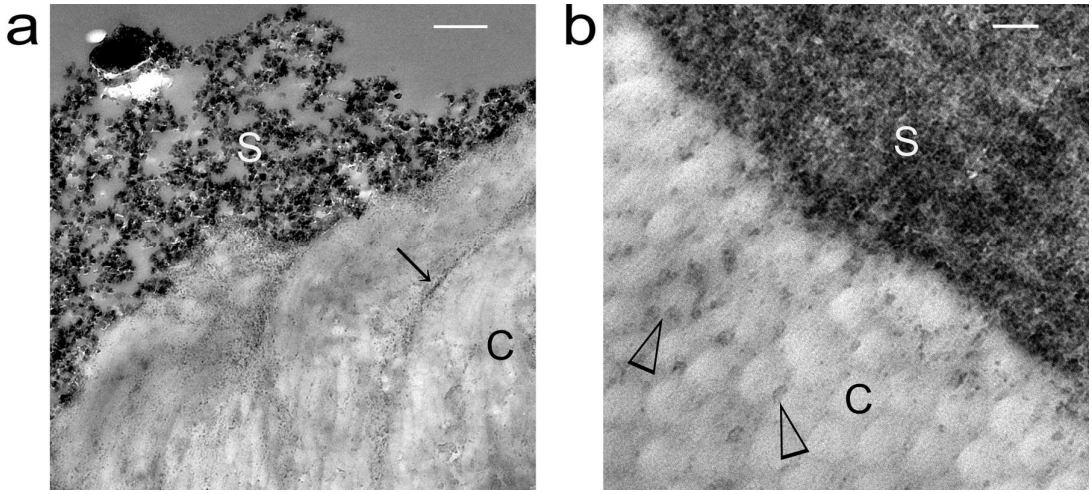

Figure S6. Unstained TEM micrographs of control demineralized fish scales that were remineralized in 5% silicic acid only (without PAH) **a.** silica particles (S) were deposited predominnatly on the surface of the fish scale. Although there was some infiltration of the silicic acid into the collagen matrix (C) via the transversal canals (arrow), deposition of silica particles was extrafibrillar in nature, between the collagen fibrils. Bar = 500 nm. **b**. High magnification image showing silica deposition in the extrafibrillar spaces (open addowheads) of the collagen fibrils (C). Intrafibrillar silica deposition was completely absent. S: silica deposits along the surface of the fish scale. Bar = 100 nm.

S7: Silicification of bovine trabecular bone

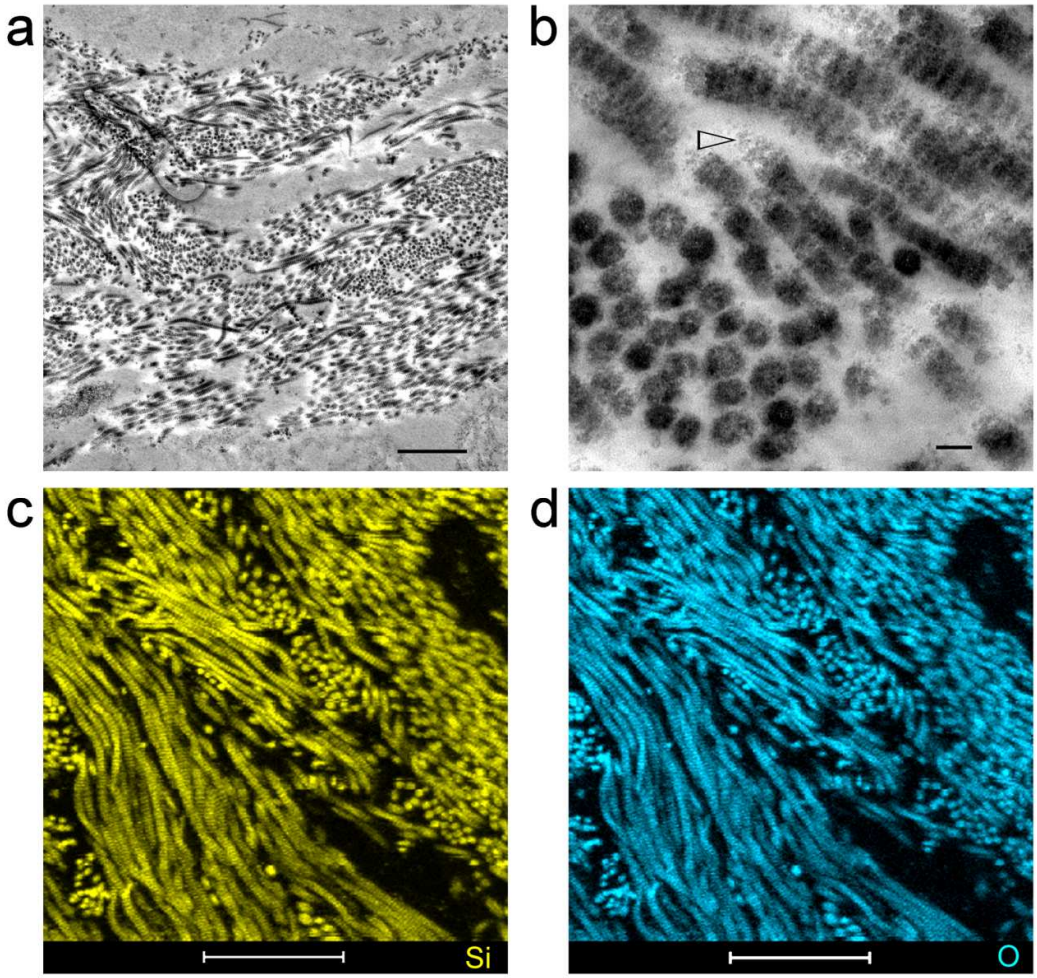

Figure S7. TEM imaging and STEM-EDX analysis of an unstained section of silicified bovine trabecular bone. STEM-EDX was performed using a non-osmicated section, **a.** Low magnification TEM of silicified bone trabeculae. Trabecular bone is less dense than the cortical bone with more spaces between the collagen fibrils (bar = 2 μm). **b**. High magnification of the silicified collagen fibrils, showing the presence of intrafibrillar silica nanoparticles (arrowhead) (bar = 100 nm). Silicon and oxygen are predominantly identified within the collagen fibrils (**c** and **d**) (bar = 2 μm). Calcium and phosphorus were absent from the silicified collagen matrix.

S8: 3-D reconstruction of silicification of demineralized bovine bone

A movie prepared from the 3-D reconstructed images visibly could be found at: http://youtu.be/k_2g9RD7xJQ, showing that the entire piece of the demineralized bone matrix was silicified.

S9: Thermogravimetric analysis of completely demineralized bovine bone

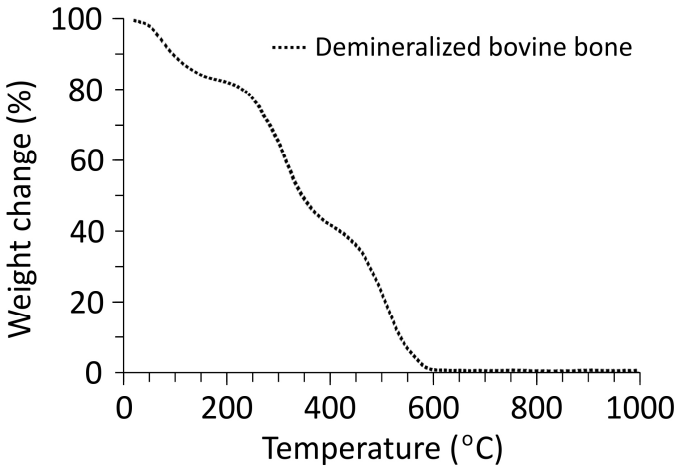

Figure S9. Thermogravimetric analysis of the demineralized bovine bone employed for silicification. The plot of weight loss *vs* temperature indicates complete weight loss after the matrix was sintered to approximately 600 °C in atmospheric air. This indicates that the originally mineralized bone was completely demineralized prior to remineralization with silica.

S10: Additional references

S1 Zylberberg, L.; Nicolas, G. *Cell. Tissue Res.* **1982**, *223*, 349-367.
S2 Kröger, N.; Lorenz, S.; Brunner, E.; Sumper, M. *Science* **2002**, *298*, 584-586.
S3 Kröger, N.; Poulsen, N. *Annu. Rev. Genet.* **2008**, *42*, 83-107.
S4 Annenkov, V. V.; Danilovtseva, E. N.; Pal'shin, V. A.; Aseyev, V. O.; Petrov, A. K.; Kozlov, A. S.; Patwardhan, S. V.; Perry, C. C. *Biomacromolecules* **2011**, *12*, 1772-1780.
S5 Brunner E, Gröger C, Lutz K, Richthammer P, Spinde K, Sumper M. *Appl. Microbiol. Biotechnol.* **2009**, *84*, 607-616.
S6 Annenkov VV, Danilovtseva EN, Filina EA, Likhoshway YV. *J. Polym. Sci. Part A: Polym. Chem.* **2006,** *44*, 820-827.
S7 Lefaux CJ, Mather PT. *Mater. Res. Soc.* **2004**, *2*, 461-463.